FILE COPY

REPORT SD-TR-89-71

(4)

AD-A216 115

Figures of Merit to Characterize Integrating Image Sensors:

A Ten-Year Update

E. F. CROSS and T. M. REESE
Aerophysics Laboratory
Laboratory Operations
The Aerospace Corporation
El Segundo, CA 90245

29 September 1989

Prepared for

SPACE SYSTEMS DIVISION
AIR FORCE SYSTEMS COMMAND
Los Angeles Air Force Base
P.O. Box 92960
Los Angeles, CA 90009-2960

Best Available Copy

DTIC
ELECTE
DEC 28 1989
S B D

APPROVED FOR PUBLIC RELEASE;
DISTRIBUTION UNLIMITED

89 12 28 034

This report was submitted by The Aerospace Corporation, El Segundo, CA 90245, under Contract No. F04701-85-C-0086-P00019 with the Space Systems Division, P.O. Box 92960, Los Angeles, CA 90009-2960. It was reviewed and approved for The Aerospace Corporation by W. P. Thompson, Director, Aerophysics Laboratory. Lt Anthony Cerveny was the Air Force project officer.

This report has been reviewed by the Public Affairs Office (PAS) and is releasable to the National Technical Information Service (NTIS). At NTIS, it will be available to the general public, including foreign nationals.

This technical report has been reviewed and is approved for publication. Publication of this report does not constitute Air Force approval of the report's findings or conclusions. It is published only for the exchange and stimulation of ideas.

ANTHONY CERVENY, 1LT, USAF
MOIE Project Officer
SSD/CNIS

RAYMOND M. LEONG, MAJ, USAF
MOIE Program Manager
AFSTC/WCO OL-AB

UNCLASSIFIED
SECURITY CLASSIFICATION OF THIS PAGE

REPORT DOCUMENTATION PAGE

1a REPORT SECURITY CLASSIFICATION Unclassified	1b. RESTRICTIVE MARKINGS
2a SECURITY CLASSIFICATION AUTHORITY	3. DISTRIBUTION / AVAILABILITY OF REPORT Approved for public release; distribution unlimited.
2b DECLASSIFICATION / DOWNGRADING SCHEDULE	
4 PERFORMING ORGANIZATION REPORT NUMBER(S) TR-0088(3911-13)-1	5. MONITORING ORGANIZATION REPORT NUMBER(S) SD-TR-89-71
6a NAME OF PERFORMING ORGANIZATION Laboratory Operations The Aerospace Corporation 6b OFFICE SYMBOL (If applicable)	7a. NAME OF MONITORING ORGANIZATION Space Systems Division
6c. ADDRESS (City, State, and ZIP Code) El Segundo, CA 90245	7b ADDRESS (City, State, and ZIP Code) Los Angeles Air Force Base Los Angeles, CA 90009-2960
8a. NAME OF FUNDING / SPONSORING ORGANIZATION 8b OFFICE SYMBOL (If applicable)	9 PROCUREMENT INSTRUMENT IDENTIFICATION NUMBER F04701-85-C-0086-P00019
8c. ADDRESS (City, State, and ZIP Code)	10 SOURCE OF FUNDING NUMBERS PROGRAM ELEMENT NO / PROJECT NO. / TASK NO. / WORK UNIT ACCESSION NO

11 TITLE (Include Security Classification)
Figures of Merit to Characterize Integrating Image Sensors: A Ten-Year Update

12 PERSONAL AUTHOR(S)
Cross, Edward F., and Reese, Thomas M.

13a TYPE OF REPORT	13b. TIME COVERED FROM _____ TO _____	14. DATE OF REPORT (Year, Month, Day)	15 PAGE COUNT
		1989 September 29	37

16 SUPPLEMENTARY NOTATION

17 COSATI CODES			18 SUBJECT TERMS (Continue on reverse if necessary and identify by block number)
FIELD	GROUP	SUB-GROUP	Camera tube performance; Imagery figures of merit; Image sensors; Television performance standards; Image standards; Vidicon standards

19 ABSTRACT (Continue on reverse if necessary and identify by block number)

A ten-year update is presented on performance criteria and measurement techniques to evaluate integrating image sensors. The integrating image sensor has an irradiance-sensitive focal plane that continuously monitors the field of view and an electronic mechanism that sequentially reads out the integrated signal on each resolution element. Ten years ago, camera tubes were the integrating imagers of interest; today, staring focal plane arrays have supplanted camera tubes as integrating imagers. The adaptability of the 1978 figures of merit to the new staring devices is reviewed and, when indicated, the figures are modified.

20. DISTRIBUTION / AVAILABILITY OF ABSTRACT ☒ UNCLASSIFIED/UNLIMITED ☐ SAME AS RPT. ☐ DTIC USERS	21. ABSTRACT SECURITY CLASSIFICATION Unclassified
22a NAME OF RESPONSIBLE INDIVIDUAL	22b TELEPHONE (Include Area Code) / 22c OFFICE SYMBOL

DD FORM 1473, 84 MAR — 83 APR edition may be used until exhausted. All other editions are obsolete.

SECURITY CLASSIFICATION OF THIS PAGE
UNCLASSIFIED

18. SUBJECT TERMS, Continued

Camera-tube standards
Staring array performance
Focal plane array standards

CONTENTS

I. INTRODUCTION AND BACKGROUND 5

II. GENERAL APPROACH AND TERMINOLOGY 7

A. TRANSFER CHARACTERISTICS 11

B. SPATIAL RESPONSE 13

C. SPECTRAL RESPONSE 24

D. UNIFORMITY OF RESPONSE 28

E. IMAGE RETENTION 28

III. SUMMARY 31

REFERENCES 33

APPENDIX: CALCULATION OF SIGNAL IRRADIANCE AT THE FOCAL PLANE WINDOW (H_s) 35

QUALITY INSPECTED 2

Accession For
NTIS GRA&I ☑
DTIC TAB ☐
Unannounced ☐
Justification
By
Distribution/
Availability Codes
Dist | Avail and/or Special
A-1

FIGURES

1. Typical video output on line-selector oscilloscope..... 9

2. Video diagram of irradiance levels on line-selector oscilloscope..... 10

3. Typical curve of transfer characteristics..... 12

4. Curve of integration element size..... 15

5. Image spot coverage by a focal-plane line array..... 16

6. Image spot coverage for a symmetrical detector-element configuration..... 18

7. Measurement for separation of two subaperture spots..... 20

8. Test for separation of two A_e image spots--50% fill-factor array 22

9. Measurements of square-wave response..... 23

10. Test for separation of two subaperture spots for a 100% fill-factor array..... 25

11. Schottky IRCCD mosaic with lenticulated faceplate..... 26

12. Subaperture image spot tests for detector arrays..... 27

13. Typical curve for spectral response measurements..... 29

I. INTRODUCTION AND BACKGROUND

Eleven years ago at The Aerospace Corporation, figures of merit were formulated to evaluate and compare the performance of television cameras. The cameras are integrating image sensors having a light-sensitive surface that continuously monitors the field of view and an electronic mechanism that sequentially reads out the integrated signal on each detector element. Laboratory test procedures and measurable parameters were established to accurately define the radiometric spatial, spectral, and gradient characteristics for this family of imaging devices. The resulting techniques and criteria were presented in 1978 at the SPIE 22nd International Technical Symposium.[1] A significant portion of the terminology and measurement techniques described in this report was taken from publications of the IRIS Specialty Sub-Group on Infrared Camera Tube Standards,[2,3] in which The Aerospace Corporation was a participant.

Ten years ago, the performance characterizations were for evaluating most integrating image sensors. Emphasis then was placed on the applicability of those characterizations to vidicon-type camera tubes. Now, a decade later, the integrating image sensor of interest is the staring focal plane array, in which a solid-state switch has replaced the slow-velocity electron beam as the electronic readout mechanism. This report discusses the adaptability of the 1978 technical approach to state-of-the-art staring arrays and modifies certain evaluation techniques to more accurately measure figures of merit for the all-solid-state devices.

Most contemporary staring detector arrays differ from camera tubes of the previous decades: the light-sensitive surface consists of discrete detector elements rather than a sensing-layer continuum, as with vidicons. Another major difference is that many detector arrays have optical and electronic elements installed as integral parts of the focal plane. These two differences in the array structure will most significantly affect performance criteria for spatial response.

In Section II, the ten-year-old approach and terminology for determining figures of merit for staring image sensors are updated, and the definitions and test procedures previously formulated for the five measurable parameters--transfer characteristics, spatial response, spectral response, uniformity of response, and image retention--are reviewed and modified in relation to staring focal plane arrays. Findings are presented in the Summary, Section III.

II. GENERAL APPROACH AND TERMINOLOGY

The integrating image sensor is treated as a black box that produces output signals corresponding to the scene at the optical image plane. Figures of merit derived for each image sensor are independent of related equipment, such as optics and video electronics. However, in many detector array configurations, the video preamplifiers are part of the focal plane structure. Windows of separate dewar assemblies for cooling the image sensor are included with the optics, unless the dewar is an integral part of the image-sensor construction. Faceplates and optical filters installed on the focal plane are considered intrinsic components of the integrating image sensor.

Operating voltages and currents that control image quality must be held constant during all the tests. Because selected image-sensor characteristics can be optimized at the expense of others, it is recommended that performance measurements be taken at more than one set of operating conditions. Such measurements aid in describing trade-offs for the comparative evaluation of various types of image sensors.

The terms sensing layer and focal plane refer to the sensitive area of the image sensor. The operating point of the sensing layer is determined from sensing-layer voltage and current ($V_{s\ell}$ and $I_{s\ell}$), measured with a dc voltmeter and dc nanoammeter, respectively.

The input irradiance (H_i) is defined as the power density at the image plane. It constitutes the total of the irradiance levels from the environment, background, and signal source. The signal irradiance at the focal plane window (H_s) is the portion of the H_i that originates from the signal source. Transmission efficiencies of external filters that may be necessary for proper performance evaluation are not considered part of the image sensor. The equations for calculating H_s based on the given test parameters are presented in the Appendix.

All video-signal measurements are obtained by monitoring the line video with a line-selector oscilloscope, as illustrated in Fig. 1. Television monitors or equivalent video-display devices can be used to qualitatively adjust image-sensor performance but not to determine measurable parameters.

The relationship between the output video signal and the input irradiance H_i is influenced by several factors. The most significant operating parameter is the value for sensing-layer current ($I_{s\ell}$), which corresponds to the monitored $V_{s\ell}$ on the line-selector oscilloscope. Figure 2 is an idealized representation of the line-selector oscilloscope waveforms for various conditions. Note that all signal amplitudes are measured from the mean value of the high-frequency fluctuations (V_{en}), whereas output voltage levels on the ordinate are directly related to irradiance levels. The three video voltage levels produced by dark, environmental, and background conditions are indicated in Fig. 2 and are defined below.

Under dark conditions, the image-sensor window is covered by an opaque reflecting cap held at the sensing-layer temperature. The resulting voltage, monitored on the line-selector oscilloscope, is the <u>dark voltage</u> (V_d).

Under environmental conditions, the image-sensor window is covered by an opaque, nonreflecting cap at the ambient temperature, which is usually approximately 300 K. The voltage monitored on the line-selector oscilloscope is the <u>environmental voltage</u> (V_e). For uncooled image sensors, V_e is zero.

For the signal-plus-background condition, all opaque caps are removed and the background and signal voltages (V_b and V_s) are produced on the line-selector oscilloscope. If a narrow-band filter at the sensing-layer temperature is placed in front of the image-sensor window so that $V_b = V_e = 0$, V_d is the no-signal voltage on the line-selector oscilloscope.

Noise, as used in these image-sensor measurements, is the random statistical fluctuations in the video output that are part of the fixed-pattern characteristics. Thus, shading signals or spot imperfections are

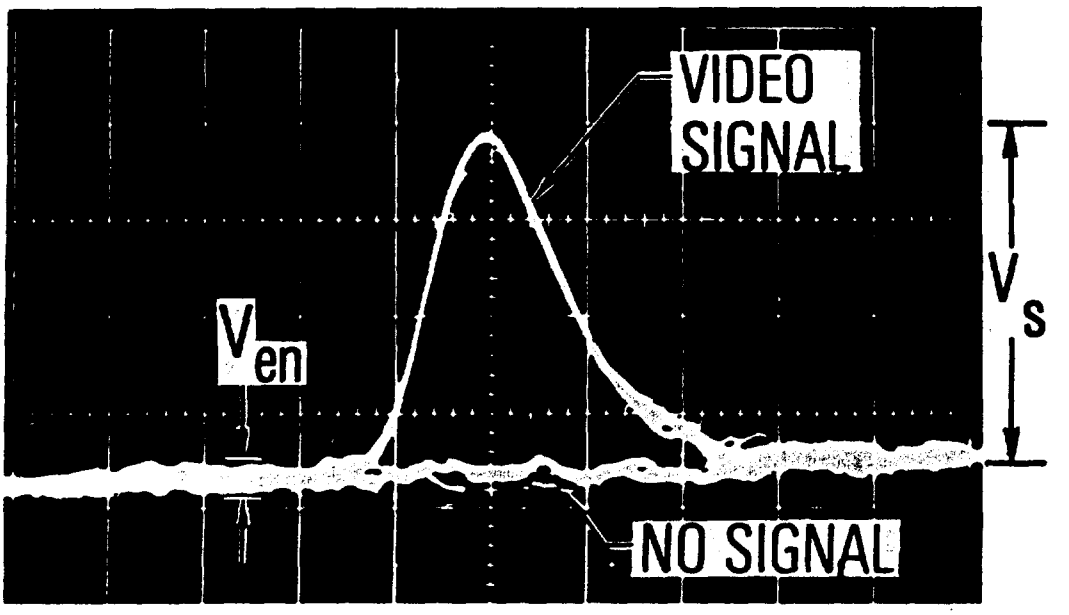

Fig. 1. Typical video output on line-selector oscilloscope.

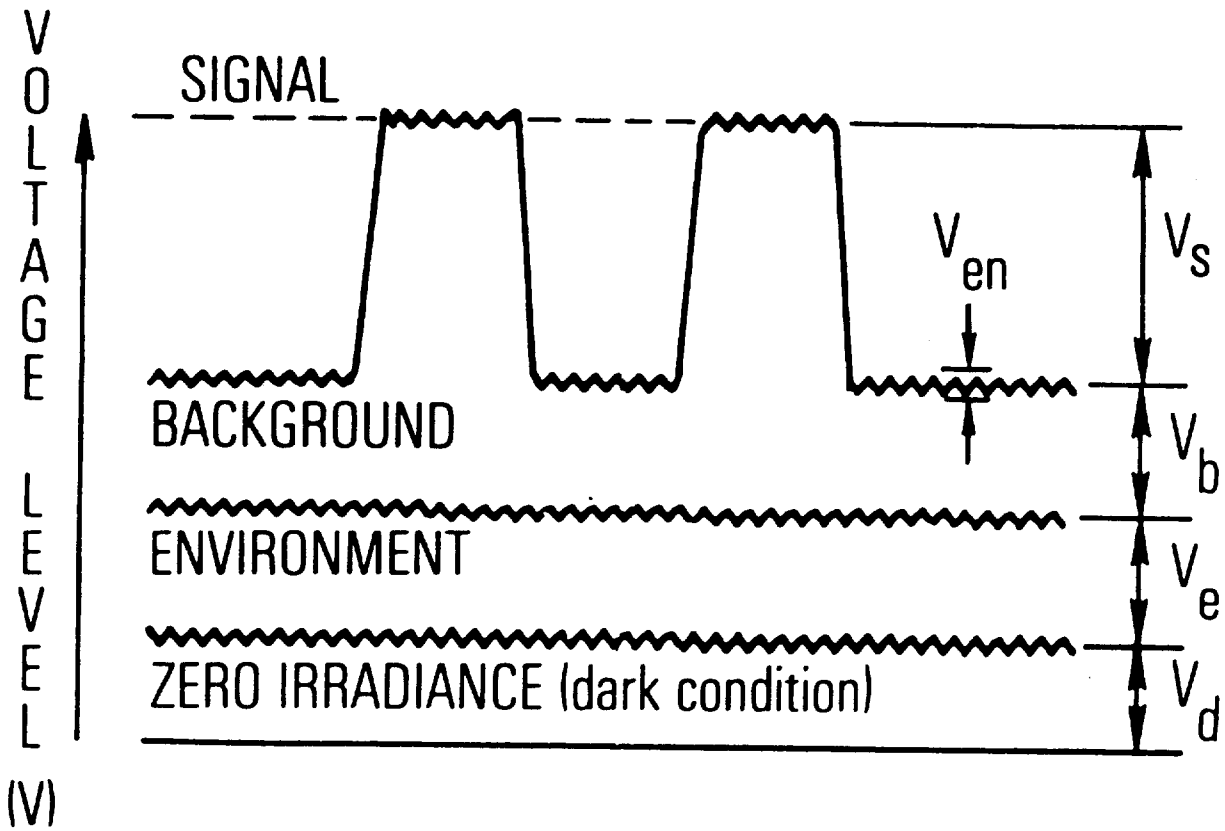

Fig. 2. Video diagram of irradiance levels on line-selector oscilloscope.

not considered part of the noise, but video fluctuations caused by such factors as sensing-layer granularity, crosstalk between adjacent elements, and elemental switching disturbances are included with noise observed on the line-selector oscilloscope. The resulting composite noise observed on the scope is non-Gaussian and cannot be easily expressed as a root-mean-square value. For the image-sensor measurements discussed below, noise is defined as the peak-to-peak envelope of high-frequency voltage fluctuations V_{en} viewed on the line-selector oscilloscope.

Five measurable parameters that can be used to describe the performance of the integrating image sensor are (1) transfer characteristics, (2) spatial response, (3) spectral response, (4) uniformity of response, and (5) image retention. The significance of and measurement techniques for each parameter are discussed in the following subsections for both camera tubes and staring focal plane arrays.

A. TRANSFER CHARACTERISTICS

Transfer characteristics relate signal irradiance at the image plane to the output signal, V_s/V_{en}, of the image sensor. The image size selected is significantly larger than the resolving element size for the image sensor. The temperature of the source is usually held constant, and neutral-density filters of known transmissions are placed in front of the blackbody aperture. In this manner, a wide range of V_s/V_{en}'s is readily produced without changing the blackbody temperature. The H_s can be calculated for each V_s/V_{en} value.

Measurements of transfer characteristics are presented as a log-log plot of H_s versus V_s/V_{en}. The linear slope of the resultant curve (γ) is expressed as

$$\gamma = \frac{d\left(\log V_s/V_{en}\right)}{d\left(\log H_s\right)} \tag{1}$$

For most image sensors, γ has a value between 0.9 and 1.0. A typical transfer characteristics curve is shown in Fig. 3. The H_s that produces a

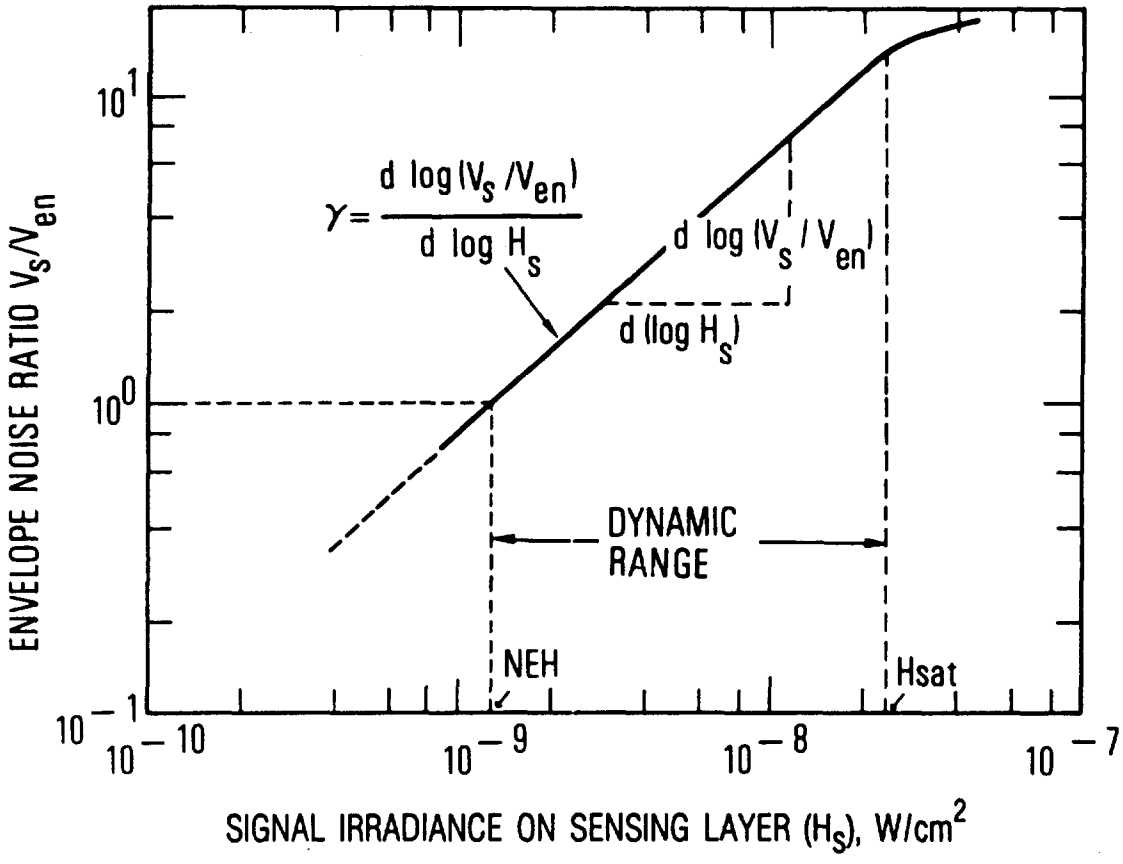

Fig. 3. Typical curve of transfer characteristics.

V_s/V_{en} of one is defined as the noise equivalent irradiance (NEH). The derived quantity NEH is a single value for specifying threshold detectivity for a given integrating image sensor. The dynamic range (DR) is defined as the saturation [H_s(sat)] to NEH ratio, expressed

$$DR = \frac{H_s(sat)}{NEH} \tag{2}$$

The derived quantity DR specifies the range of irradiance levels that a given integrating image sensor can view simultaneously.

B. SPATIAL RESPONSE

Spatial response or resolution describes camera-system fidelity in converting image size and pattern at the focal plane to an output video signal. Experience has shown, however, that no single measurable parameter can concisely define resolution for all types of integrating image sensors. The three spatial-response criteria that have been established over the past 25 years are (1) integration element size, (2) separation of two subaperture spots, and (3) square-wave response. All three provide reliable measures for comparative image-sensor evaluation.

The staring detector array consists of discrete sensing elements separated by nonactive gaps (dead zones); therefore, optimal image-resolving power is determined by detector element size and dead-zone dimensions. Spatial response characteristics described in the following paragraphs provide the calculated values that represent the optimal realizable performance. Discrepancies between the analytically derived values and measured data can be attributed to response nonuniformities across the detector array, imperfections in the on-chip electronics, and electronic/optical crosstalk between adjacent sensing elements.

Integration element size defines image-sensor response to incident radiant power as image size is decreased to subelement dimensions while

video signal output is held constant ($V_s/V_{en} = K$). For this measurement, a mask with variable-sized circular apertures is placed in front of a blackbody source. The initial aperture size focused on the image plane should be at least twice as large as the anticipated focal plane resolution. A blackbody temperature is selected that produces a V_s/V_{en} in the range between 5 and 10 to monitor on a line selector. As the aperture size is reduced, V_s/V_{en} remains constant until the image dimensions approach the integration element size of the image sensor. From that point, the blackbody irradiance is increased to keep V_s/V_{en} constant as the blackbody aperture is made smaller.

The optical, aperture, and blackbody parameters are known, so the image area and irradiance at the focal plane (A_i and H_s) can be calculated. A typical log-log plot of $A_i H_s$ in watts as a function of A_i in square centimeters is shown in Fig. 4. For the segment of the curve at a constant slope of one, the V_s/V_{en} corresponding to H_s remains constant even though A_i is decreasing with small-aperture-size selection. The abscissa value where this curve changes abruptly from 45° to a much smaller angle is defined as the <u>area of minimum integration element size</u> (A_e). The product of NEH, derived in Subsection II.A, and A_e yields an element sensitivity figure of merit in watts per integration element size (P_e^*).

For focal plane arrays, the optimal A_e that can be realized can be calculated from the array's fill factor and elemental detector dimensions before laboratory measurements are performed. An array configuration in which each detector row is separated by a dead-zone area of comparable size is diagramed in Fig. 5. In Fig. 5a, the image spot size on the light-sensitive surface is just large enough in diameter to always totally encompass at least two square detector elements when the image spot center is located midway between adjacent rows or columns of detector elements. The minimum image spot diameter (d_e') for this condition, based on focal plane geometries, is expressed mathematically as

$$d_e' = \sqrt{(2w+\ell)^2 + (2w+s)^2} \qquad (3)$$

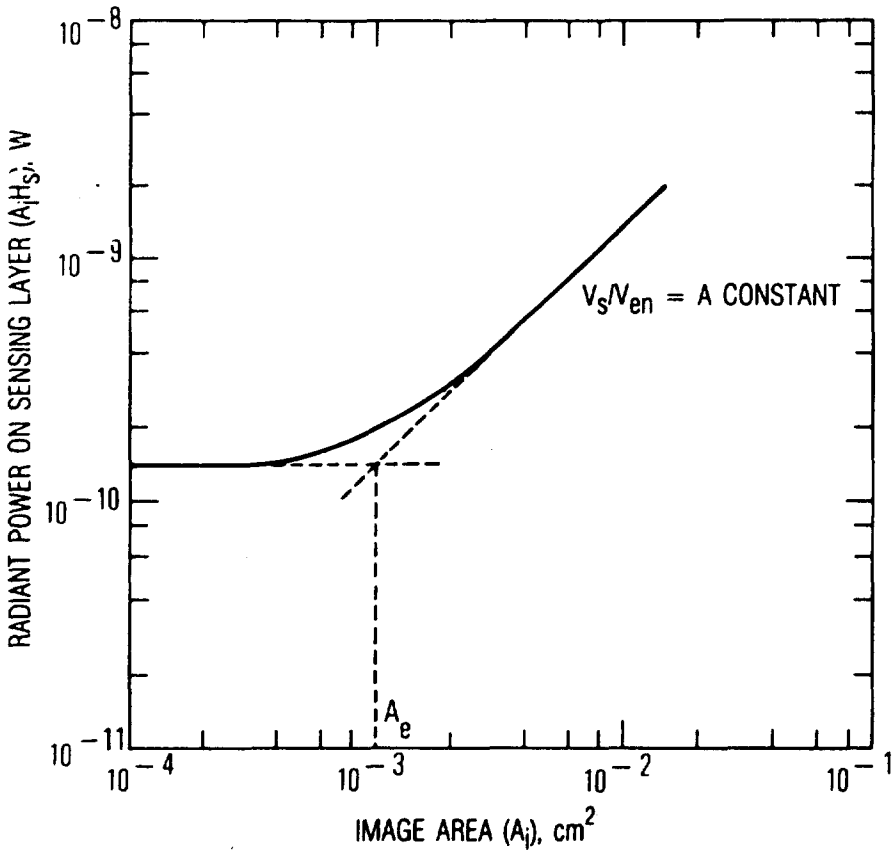

Fig. 4. Curve of integration element size.

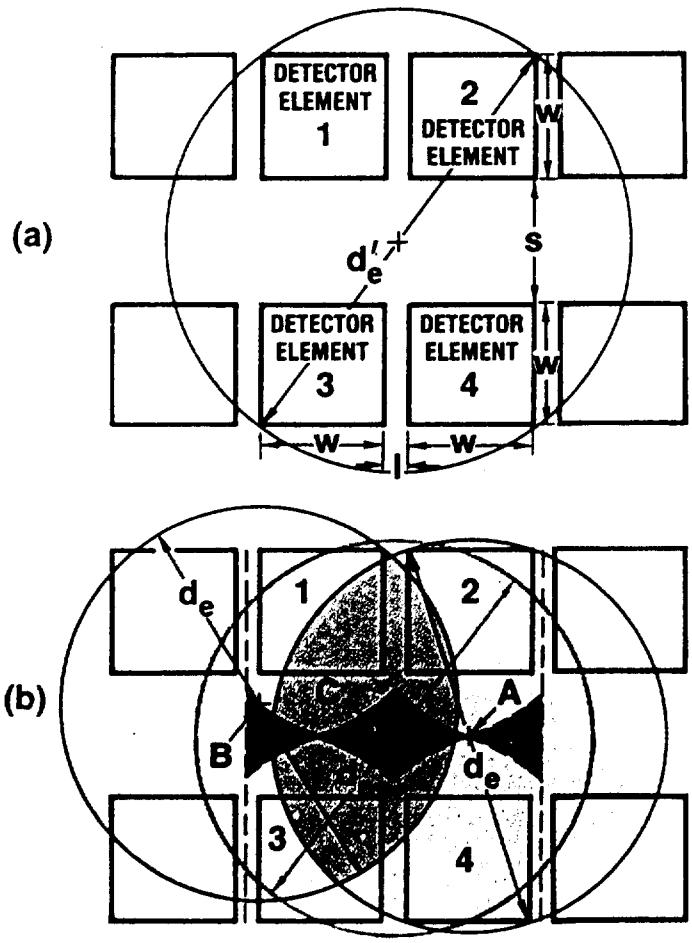

- IMAGE SPOT CENTERED AT DEAD ZONE CENTROID d_e'
- DETECTOR ELEMENTS 1, 2, 3 AND 4, TOTALLY COVERED FOR $d_i = d_e'$
- FOR $d_i < d_e'$ AT THIS CENTER LOCATION NO ELEMENT IS TOTALLY COVERED

IMAGE SPOT DIAMETER d_e

CENTER LOCATION	DETECTOR ELEMENT TOTALLY COVERED
A	2 AND 4
B	1
C	NONE

FOCAL PLANE AREAS WHERE IMAGE SPOTS WITH $d_i = d_e$ DO NOT TOTALLY COVER ANY DETECTOR ELEMENT

Fig. 5. Image spot coverage by a focal-plane line array.

where

w = width and length of a square sensing element,

ℓ = width of the nonactive area (dead zone) between columns of sensing elements,

s = width of the nonactive area (dead zone) between rows of sensing elements.

Then $A_e' = \pi/4\ (d_e')^2$, where A_e' corresponds to an image size large enough to totally cover at least one detector element no matter where the circle's center falls on the focal plane.

This A_e' is the limiting factor only when the image spot is centered exactly at the dead-zone centroidal point. The probability is remote that any image spot will be centered exactly at this point, and it is extremely remote that such imagery would remain absolutely stationary for several integration times. Therefore, a more meaningful approach for establishing A_e is to decrease image diameter (d_i) to the point where 90% of spot center locations totally cover at least one detector element. Figure 5b diagrams three typical image locations for $d_i = d_e$ and $d_e < d_e'$. The image spot centered at point A totally covers two detector elements, whereas d_e centered at point B totally covers only one element. For d_e centered at point C or any other point in the shaded dead-zone areas, no detector element is covered totally.

A focal-plane example for which dead-zone area is the same as in the preceding example, but distributed equally on all sides between adjacent detectors, is diagramed in Fig. 6. We analyze it to determine whether spatial response for subaperture imagery improves. In Fig. 6a, image spot size on the light-sensitive surface is just large enough in diameter to always totally encompass at least two detector elements independent of location on the focal plane. The minimum image spot diameter (d_e'), with equal dead-zone area ($\ell = s$), is given by

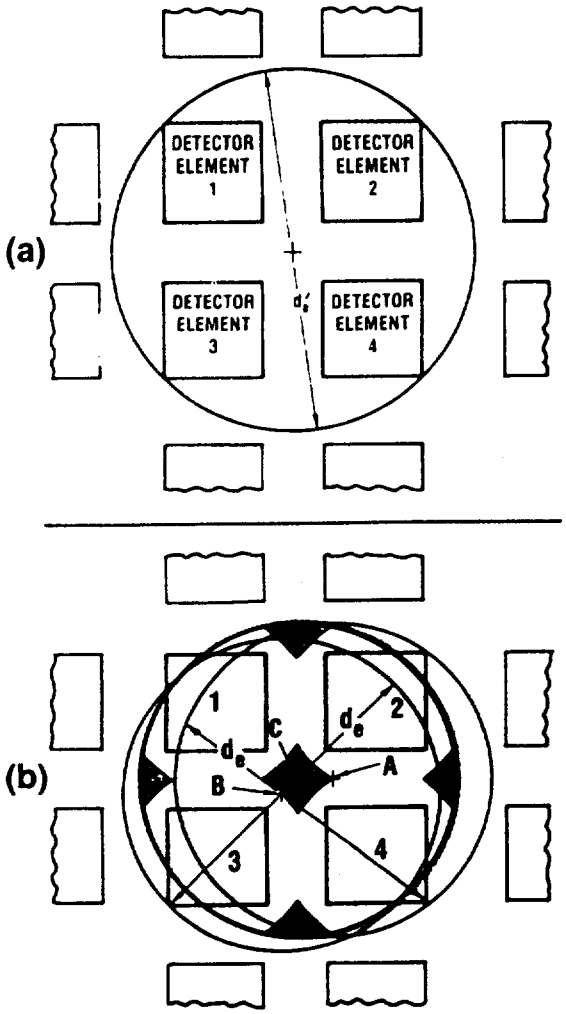

- IMAGE SPOT WITH $d_i = d_e'$
- FOUR DETECTOR ELEMENTS ARE TOTALLY COVERED

FOCAL PLANE DATA

- SQUARE DETECTOR ELEMENTS $w \times w$
- ALL DEAD ZONE AREAS $s \times w$ WITH $s = w/2$

IMAGE SPOT WITH $d_i = d_e < d_e'$

CENTER LOCATION	DETECTOR ELEMENT TOTALLY COVERED
A	2 AND 4
B	3
C	NONE

FOCAL PLANE AREAS WHERE IMAGE SPOTS WITH $d_i = d_e$ DO NOT TOTALLY COVER ANY DETECTOR ELEMENT

Fig. 6. Image spot coverage for a symmetrical detector-element configuration.

$$d_e' = \sqrt{2}\ (2w+s) \tag{4}$$

and

$$A_e' = \frac{\pi}{2}\ (2w+s)^2 \tag{5}$$

Figure 6b diagrams three typical image spot locations for $d_i = d_e$ and $d_e < d_e'$. The image spot coverage of detector elements is the same as in Fig. 5b.

The array examples depicted in Figs. 5 and 6 and discussed in the preceding paragraphs have fill factors in the 50% range. For both examples, A_e was calculated to be approximately 25% smaller than A_e'. These results indicate that the fill-factor percentage is more significant for d_e than is distribution of dead-zone areas.

For image sensors with a light-sensitive focal plane that is a continuum, the separation of two subaperture spots measures the video output modulation as the spacing between adjacent point images at the sensing surface is varied and V_s/V_{en} is held at a constant value, of the order of 10 to 15. For this test, masks having two circular apertures of equal size and variable spacings were placed in front of the blackbody source. The subaperture mask is designed to produce spot image pairs at the focal plane that are significantly smaller than A_e and have centerline spacings that can be varied over approximately an order of magnitude. As shown in Fig. 7a, the <u>differential modulation voltage</u> (V_M), corresponding to the midpoint between two subaperture images, is measured for each mask setting until the V_M is no longer discernible (i.e., $V_M = 0$). The ratio of V_M to V_s is defined as the <u>modulation</u> (M), and it is dimensionless.

On the bases of known optical parameters and spot separation distances, the reciprocal of centerline distances between images ($1/d_s$) is calculated for each M. Figure 7b is a typical Cartesian coordinate plot of the variation of M in percentage as a function of $1/d_s$ in lines per millimeter.

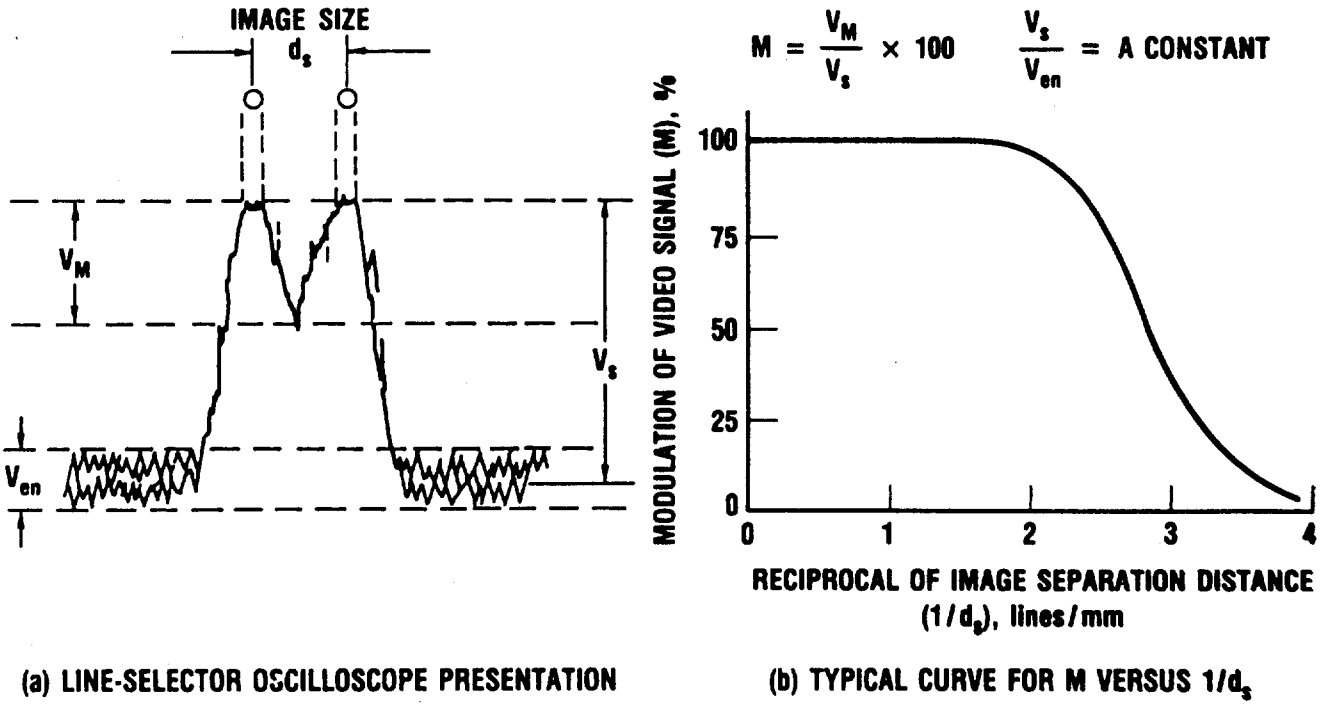

(a) LINE-SELECTOR OSCILLOSCOPE PRESENTATION

(b) TYPICAL CURVE FOR M VERSUS $1/d_s$

Fig. 7. Measurement for separation of two subaperture spots.

For image sensors consisting of discrete detector elements separated by dead zones (i.e., fill factor less than 90%), it is difficult to reliably measure the separation of two subaperture spot images. This problem results from (1) the inability to always position the subaperture pair so that each spot falls completely on a sensing element, and (2) the adjustment needed for large V_M/V_s fluctuations produced by the changing spot locations relative to the dead-zone gap. For arrays with under 90% fill factor, the separation of two A_e spot images (not subaperture) provides the most definitive resolution criterion for this spot pair imagery. Figure 8 diagrams three examples of two A_e spot images on a balanced 50% fill-factor array. The modulation M in Fig. 8a decreases to 65% (Fig. 8b) and 43% (Fig. 8c) as the centerline distances between spot images become smaller. The heavily shaded areas on the intervening detector elements correspond to the radiant intensity that decreases the amount of observable voltage modulation (V_M).

The third spatial-response criterion, the square-wave response, is the measurement of output video modulation from the image sensor as spacings between bar-pattern images at the sensing layer are varied while H_s is held constant. Each mask in a series of bar-pattern masks is set in front of a blackbody source, and the resulting modulated V_s/V_{en} is measured on a line-selector oscilloscope, as shown in Fig. 9a. The modulation M decreases with reduced bar-pattern width after remaining relatively constant for the initial large pattern widths.

The square-wave amplitude response is given as a plot of M in percentage as a function of line number per millimeter. The line number is the reciprocal of the width between pairs of imaged bars on the sensing layer (N). Figure 9b is a typical plot of square-wave-response Cartesian coordinates, with M the ordinate and N the abscissa.

For an image sensor consisting of a discrete detector array with less than 90% fill factor, the decreasing M values are not easily established because the individual voltage peaks and valleys after each bar pattern will fluctuate significantly. This inconsistency in measurements of M is

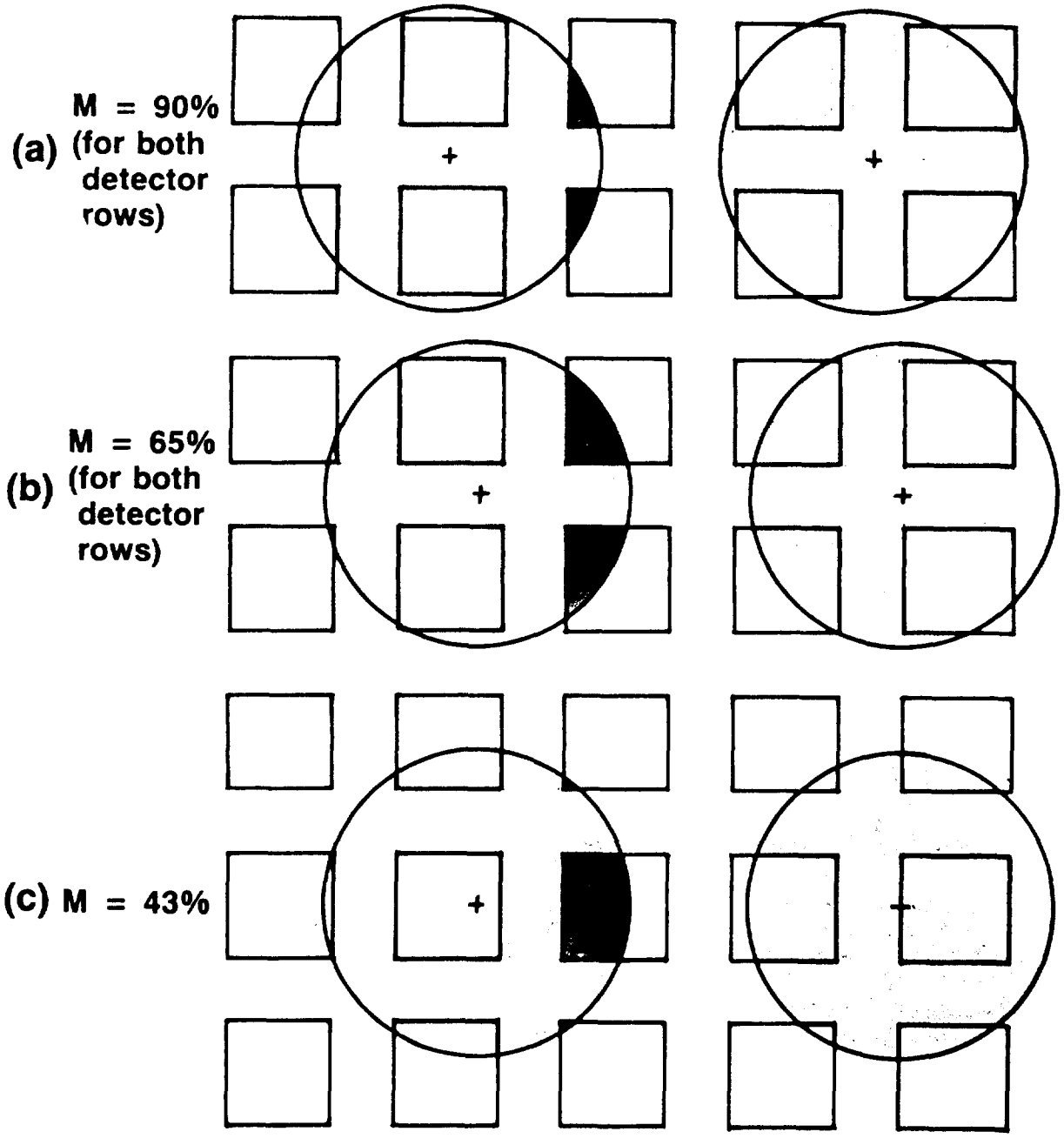

Fig. 8. Test for separation of two A_e image spots--50% fill-factor array.

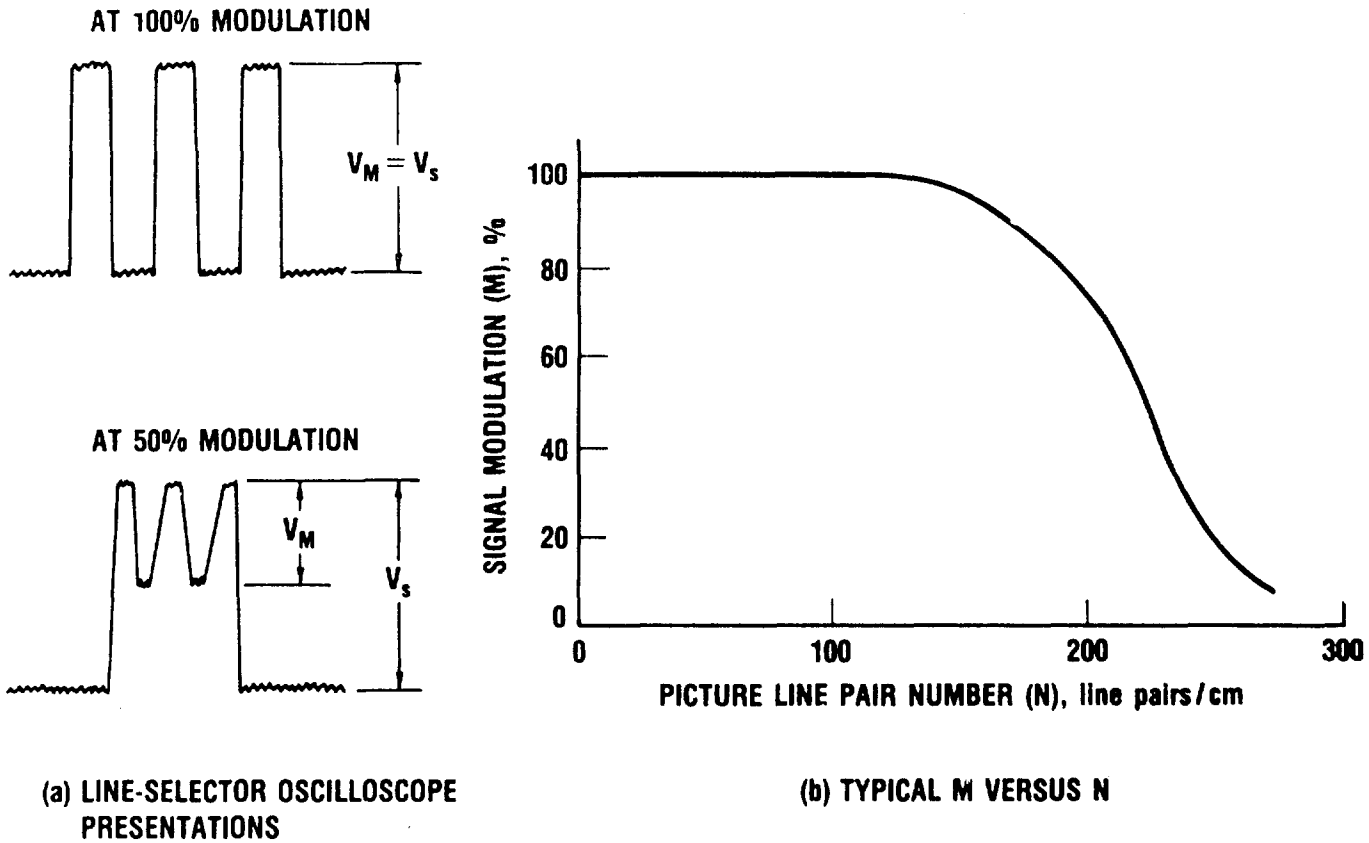

Fig. 9. Measurements of square-wave response.

caused by the individual bar and slot images falling on different dead-zone and detector-area segments.

If the image sensor consists of a detector array with over 90% fill factor, the sensitive surface approximates a continuum, as with vidicons, but limiting resolution is precisely related to detector element dimensions. This high fill factor can be obtained with bump-bonding construction or by installing a lenticulated faceplate on the detector array so that all focused irradiance is directed to an active area on the focal plane. For 100% fill-factor arrays, Fig. 10 diagrams the two-subaperture spot imagery as separation distances are made smaller.

An illustration of the Schottky IRCCD array with a lenticulated faceplate installed over the front surface is presented in Fig. 11. This array has an unbalanced dead-zone distribution as described in Fig. 5 and a fill factor of approximately 40%. Figure 12 plots separated spot-image curves for an IRCCD array with and without the lenticulated faceplate (i.e., 85% and 40% fill factors). As expected, the lenticulated configuration began to decrease from a 100% modulation at a slightly longer d_s than did the unlenticulated array. However, the faceplate insertion provided a smooth and extended decrease in M, whereas the M for the unmodified focal plane dropped sharply to zero when image-separation lengths became comparable to fill-factor geometry. This difference in responses demonstrates that the two spot images can be identified at closer distances with the lenticulated faceplate on the focal plane.

C. SPECTRAL RESPONSE

Spectral response is the relationship between the spectral wavelength of signal irradiance and the output video signal. It can be defined by the magnitude of H_s required to maintain the same V_s/V_{en} as the spectral wavelength of H_s is varied. A series of narrow-band filters and a neutral-density filter magazine are placed in front of the aperture of a blackbody source that is focused on the image-sensing layer.

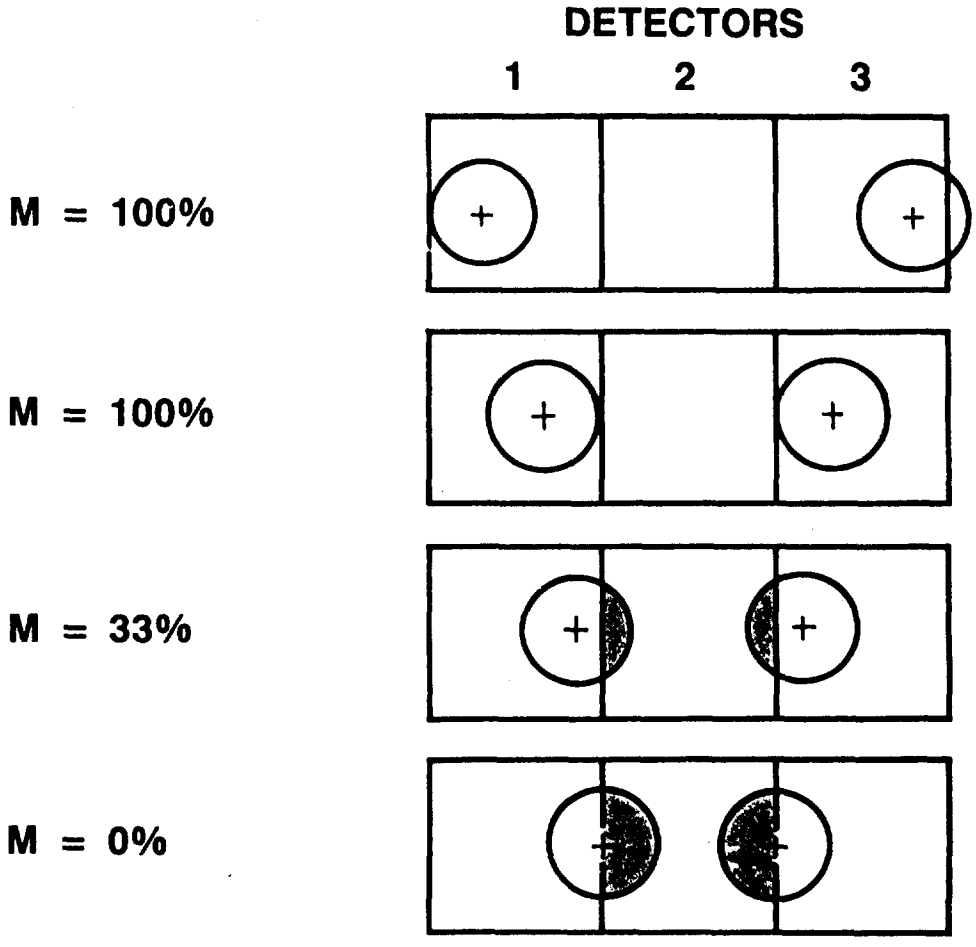

Fig. 10. Test for separation of two subaperture spots for a 100% fill-factor array.

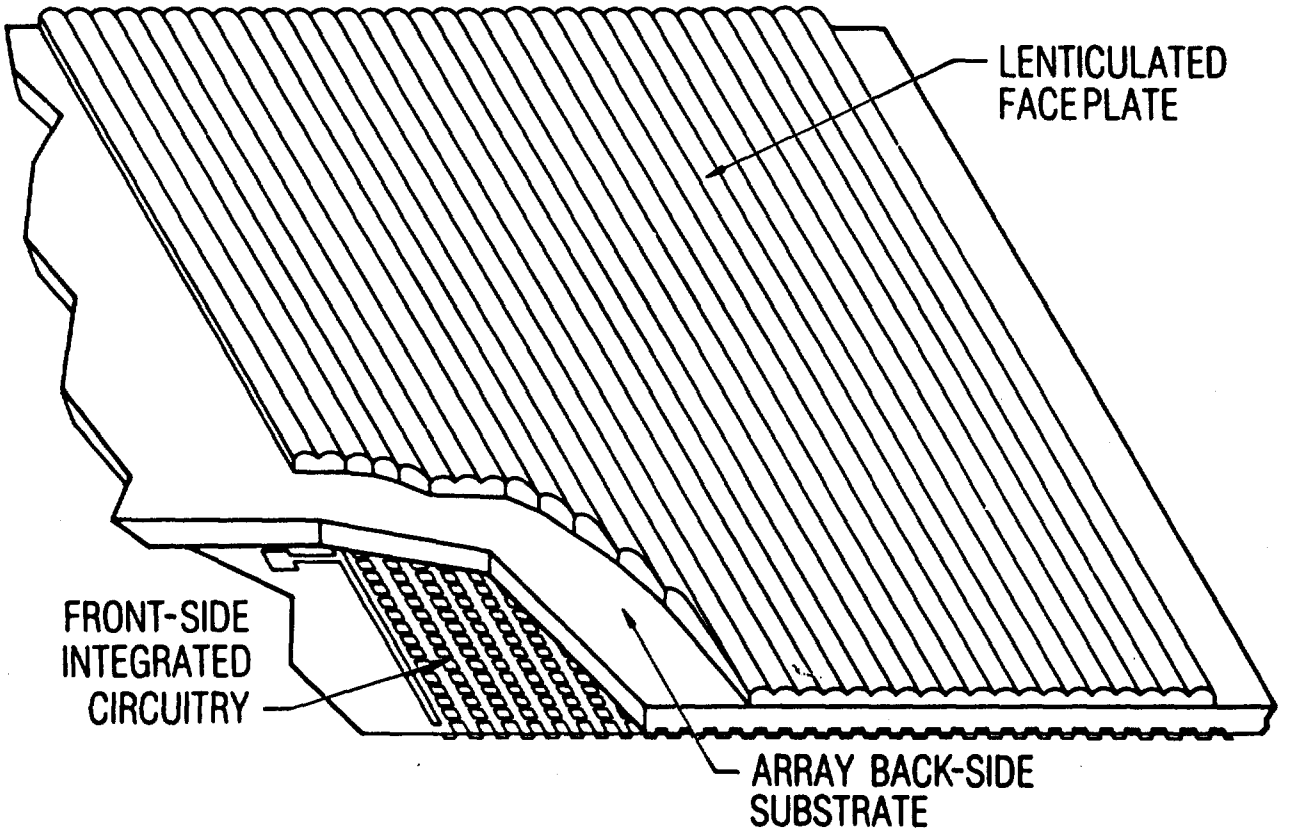

Fig. 11. Schottky IRCCD mosaic with lenticulated faceplate.

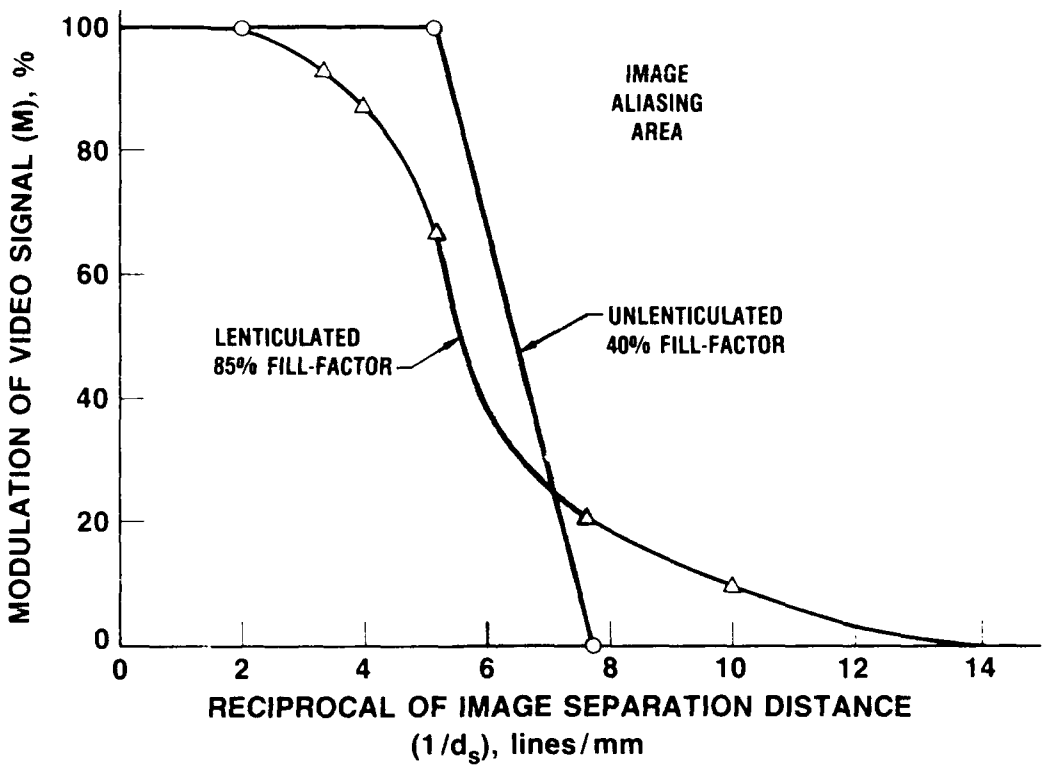

Fig. 12. Subaperture image spot tests for detector arrays.

The blackbody temperature is selected to provide a high V_s/V_{en} value through (1) a narrow-band filter that transmits in the spectral region of anticipated maximum sensitivity for the image sensor, and (2) neutral-density filters that attenuate radiant emittance from the blackbody source by almost three orders of magnitude. In this manner, the blackbody temperature can be held constant and only the neutral-density filters are changed for each selected narrow-band filter. Without modifications, this test is valid for both vidicons and focal plane arrays.

The measured spectral response data are presented as a semilog plot of the reciprocal of NEH in square centimeters per watt as a function of wavelength (λ) in microns. A typical spectral response curve is shown in Fig. 13. The NEH values were derived from the γ of the transfer characteristics curve and the measured H_s at each wavelength.

D. UNIFORMITY OF RESPONSE

Uniformity of response is the gradual variation in video output that is spatially related to the sensing-layer area. Variations are considered to be gradual if they are composed of low-frequency voltage signals less than 150 kHz when viewed on the line-selector oscilloscope. This parameter is determined by monitoring the V_s/V_{en} variations as a target of constant irradiance is positioned on various segments of the sensing layer. This method is only for image sensors that have constant γ's throughout the sensing layer, as sometimes occurs with detector-element arrays. If γ is not constant with location, as with some focal plane arrays, a transfer characteristics curve must be taken at each target location.

E. IMAGE RETENTION

Image retention is the time observed for the output video signal to decay after instantaneous removal of a signal irradiance level. This parameter also can be described in terms of the number of frame times required to erase the V_s/V_{en} corresponding to an H_s value. Irradiance from a blackbody source is set up to produce a V_s/V_{en} linear portion of the image

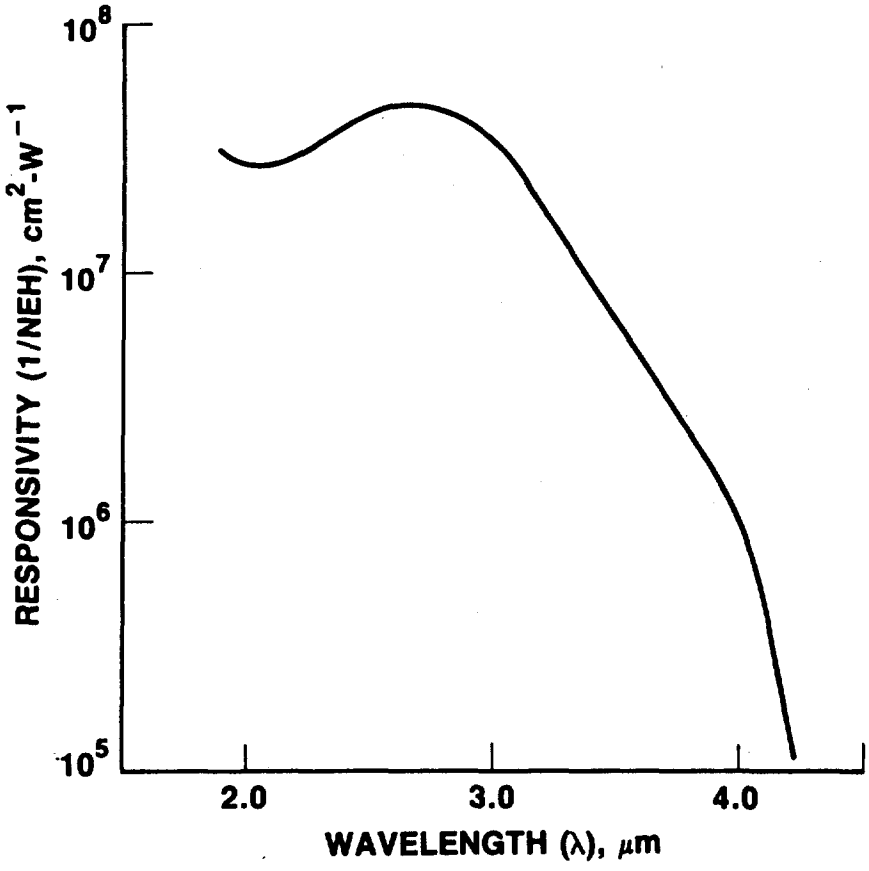

Fig. 13. Typical curve for spectral response measurements.

sensor's transfer characteristics curve. A Polaroid camera monitors the line-selector oscilloscope presentation of the target image. For many discrete detector arrays, the signal-response lag of individual sensing elements is negligible relative to the integration time, and observed image retention times in these instances are attributable to related electronics.

III. SUMMARY

The five figures of merit described here continue to be reliable criteria for evaluating integrating image sensor performance. These measurable parameters can be applied to both past and current integrating image sensors, including standard visible-light vidicons, infrared camera tubes, solid-state focal plane arrays, and charge-coupled-detector arrays. Spatial response is the only figure of merit that must be revised to accommodate detector arrays with noticeably lower fill factors. The modified test procedures require no new laboratory equipment, and the optimal resolution for discrete detector arrays can be calculated on the basis of focal-plane geometry and dimensions.

REFERENCES

1. E. F. Cross and G. I. Segal, "Figures of Merit to Characterize Integrating Image Sensors," in Modern Utilization of Infrared Technology IV, Proc. SPIE 156, 193-199 (1978).

2. "Determination of Infrared Camera Tube Characteristics: Report of the Working Panel, Specialty Group on Infrared Image-forming Sensors," Proc. IRIS 10, 49-55 (April 1966).

3. "Proposed Standards for Measurements on Infrared Camera Tube: Report of the Working Panel, Specialty Group on Infrared Image-forming Sensors," Proc. IRIS 8, 51-59 (August 1963).

APPENDIX

CALCULATION OF SIGNAL IRRADIANCE AT THE FOCAL PLANE WINDOW (H_s)

Signal irradiance at the focal plane window (H_s) is calculated from the following equation:

$$H_s = \frac{t_o t_f t_a t_n W_s}{4F^2(M + 1)^2 + 1} \qquad \text{(A-1)}$$

where

t_o = transmission of system optics
t_f = transmission of external band-limiting filter
t_a = atmospheric transmission for optical path
t_n = transmission of any neutral-density filter
W_s = radiant emittance, W/cm^2
F = f-number of the optical system
M = magnification of the optical system

Using a standard blackbody source as the calibration signal, the radiant emittance (W_s), as determined by the overall spectral bandpass of the image sensor, optics, and external spectral filters, is calculated from Planck's law:

$$W_s = 3.74 \times 10^{-12} \int_{\lambda_1}^{\lambda_2} \frac{1}{\lambda^5} \left[\exp(1.438/\lambda T) - 1\right]^{-1} d\lambda \qquad \text{(A-2)}$$

where

λ_2 = upper wavelength cutoff, cm
λ_1 = lower wavelength cutoff, cm
T = temperature of blackbody source, degrees Kelvin.

LABORATORY OPERATIONS

The Aerospace Corporation functions as an "architect-engineer" for national security projects, specializing in advanced military space systems. Providing research support, the corporation's Laboratory Operations conducts experimental and theoretical investigations that focus on the application of scientific and technical advances to such systems. Vital to the success of these investigations is the technical staff's wide-ranging expertise and its ability to stay current with new developments. This expertise is enhanced by a research program aimed at dealing with the many problems associated with rapidly evolving space systems. Contributing their capabilities to the research effort are these individual laboratories:

Aerophysics Laboratory: Launch vehicle and reentry fluid mechanics, heat transfer and flight dynamics; chemical and electric propulsion, propellant chemistry, chemical dynamics, environmental chemistry, trace detection; spacecraft structural mechanics, contamination, thermal and structural control; high temperature thermomechanics, gas kinetics and radiation; cw and pulsed chemical and excimer laser development including chemical kinetics, spectroscopy, optical resonators, beam control, atmospheric propagation, laser effects and countermeasures.

Chemistry and Physics Laboratory: Atmospheric chemical reactions, atmospheric optics, light scattering, state-specific chemical reactions and radiative signatures of missile plumes, sensor out-of-field-of-view rejection, applied laser spectroscopy, laser chemistry, laser optoelectronics, solar cell physics, battery electrochemistry, space vacuum and radiation effects on materials, lubrication and surface phenomena, thermionic emission, photosensitive materials and detectors, atomic frequency standards, and environmental chemistry.

Computer Science Laboratory: Program verification, program translation, performance-sensitive system design, distributed architectures for spaceborne computers, fault-tolerant computer systems, artificial intelligence, microelectronics applications, communication protocols, and computer security.

Electronics Research Laboratory: Microelectronics, solid-state device physics, compound semiconductors, radiation hardening; electro-optics, quantum electronics, solid-state lasers, optical propagation and communications; microwave semiconductor devices, microwave/millimeter wave measurements, diagnostics and radiometry, microwave/millimeter wave thermionic devices; atomic time and frequency standards; antennas, rf systems, electromagnetic propagation phenomena, space communication systems.

Materials Sciences Laboratory: Development of new materials: metals, alloys, ceramics, polymers and their composites, and new forms of carbon; nondestructive evaluation, component failure analysis and reliability; fracture mechanics and stress corrosion; analysis and evaluation of materials at cryogenic and elevated temperatures as well as in space and enemy-induced environments.

Space Sciences Laboratory: Magnetospheric, auroral and cosmic ray physics, wave-particle interactions, magnetospheric plasma waves; atmospheric and ionospheric physics, density and composition of the upper atmosphere, remote sensing using atmospheric radiation; solar physics, infrared astronomy, infrared signature analysis; effects of solar activity, magnetic storms and nuclear explosions on the earth's atmosphere, ionosphere and magnetosphere; effects of electromagnetic and particulate radiations on space systems; space instrumentation.